Electronic Supplementary Information

Surface engineering of cobalt carbide spheres through N, B Co-doping achieved by room-temperature in situ anchored effect for active and durable multifunctional electrocatalysts

Xinzhi Ma,[a] Kaiyue Li,[a] Xiao Zhang,[b] Bo Wei,[c] Huan Yang[a] Lina Liu,[a] Mingyi Zhang,[b] Xitian Zhang,*[b] and Yujin Chen*[a]*

[a] Key Laboratory of In-Fiber Integrated Optics, Ministry of Education and College of Science, Harbin Engineering University, Harbin 150001, China.

[b] Key Laboratory for Photonic and Electronic Bandgap Materials, Ministry of Education and School of Physics and Electronic Engineering, Harbin Normal University, Harbin 150025, China.

[c] Department of Physics, Harbin Institute of Technology, 150001, Harbin 150001, China

*Corresponding authors.

E-mail addresses: chenyujin@hrbeu.edu.cn (Y. Chen), xtzhangzhang@hotmail.com (X. Zhang), bowei@hit.edu.cn (B. Wei)

Experimental Section

Chemicals. All chemicals including cobalt (purity, >99.99%; diameter, ~0.5 μm, Aladdin Chemical Co., Ltd.), active carbon powder (purity, >99.99%; diameter, Aladdin Chemical Co., Ltd.), and $NaBH_4$ (purity, >98%; diameter, Aladdin Chemical Co., Ltd.) were of analytical grade and used as-received without further purification.

Synthesis of Co_3C and Co_3C-B. The synthesis of high-performance materials was mainly through a ball-milled method and followed a reduction reaction by $NaBH_4$. Firstly, the cobalt power and pure active carbon were mixed with a mole ratio of 1:1 and were ball-milled using a planetary ball mill (Fritsch Pulverisette 4) with the ball-to-power weight ratio of 20:1. Before ball milling, the grinding bowls were performed an Ar (99.99%) inflation−deflation process to the remove the inner air and further vacuumed the pressure of bowls to 95 Kpa. The ball milling was carried out at a rotational speed of 900 rpm/min for 10 h. Then the product was took out and dipped in 0.5 M $NaBH_4$ ethanol solution with continuous stirring for 15 hours. Many fine air bubbles were generated during the violent reaction between Co_3C particles and $NaBH_4$. Finally, the products were cleaned with alcohol and deionized water for ten times. After the vacuum filtration processes, the powder was collected and dried at room temperature.

Synthesis of Co_3C-N and Co_3C-NB. Typically, active carbon powder were placed in the middle location of a tube furnace, and then heated to 700 °C at 10 °C min-1 under a flowing NH_3 atmosphere and maintained for 3 h, and then allowed to cool to room temperature. The as-prepared N-doped active carbon powder was used as the carbon

source. For the synthesis of Co_3C-N and Co_3C-NB catalysts, the all experiment conditions are remaining the same.

Structural Characterization. X-ray powder diffraction (XRD) was performed using a Rigaku D/max2600 X-ray diffractometer with Cu-Kα radiation (λ = 1.54178 Å). The crystallite sizes of the Co_3C-based materials with different relevant data of crystal planes are calculated by Scherrer equation: D = 0.9 λ / β cosθ, where D is the crystallite size，λ is the X-ray wavelength (0.15418 nm), β is the half-maximum breadth and θ is the Bragg angle of different planes. The field-emission scanning electron microscopy (FE-SEM) images were taken on a SU 70, Hitachi, Japan The transmission electron microscopy (TEM) was performed on a FEI, Tecnai TF20 field-emission electron microscope operated at an acceleration voltage of 200 kV. X-ray photoelectron spectra (XPS) were obtained on a Thermofisher Scientific Company X-ray photoelectron spectrometer with Mg Kα as the excitation source. The nitrogen adsorption-desorption isotherms and corresponding pore size distribution were measured using an ASAP 2010 accelerated surface area and porosimetry instrument (Micromeritics). Surface area was calculated using the Brunauer-Emmett-Teller (BET) equation.

Electrochemical Activities of the Catalysts. Electrochemical measurements were carried out in a three-electrode system on a VMP3 electrochemical workstation (BioLogic，France) with a standard three-electrode electrochemical cell coupled with a RRDE 3A RRDE-3A Rotating Ring Disk Apparatus.

ORR and OER Activities of the Catalysts. To assess the ORR and OER activities of

N-Co$_3$C and Co$_3$C before and after NaBH$_4$ treatments, commercial Pt/C powers were measured using a three-electrode configuration in 0.1 M KOH at a scan rate of 10 mV s^{-1}.

These catalysts were loaded on the glassy carbon electrode (GCE) with the same loading mass of 0.353 mg cm^{-2}. For simple catalysts without CC, typically, 5 mg catalysts mixed with 50 μl Nafion solution were dispersed in 550 ml of ethanol solution and sonicated for 30 min to form a homogeneous ink. And then, 3 μl dispersion solutions were dropped onto a glassy carbon electrode with a diameter of 3 mm. Carbon rod and Ag/AgCl (3M KCl saturated) were used as counter and reference electrodes, respectively. All the electrode potential were referenced to Ag/AgCl reference electrode, which was converted to reversible hydrogen electrode (RHE) using the equation E$_{(RHE)}$ = E$_{(Ag/AgCl)}$ + 0.059 × PH + 0.198.

With regard to ORR experiment, the LSV polarization data was executed from 0.1~ –0.8V (vs. Ag/AgCl) at the scan rate of 10 mV s^{-1} under various rotating speeds (400 rpm, 625 rpm, 900 rpm, 1,225 rpm, 1,600 rpm, 2,025 rpm). The Koutecky-levich equation as below was employed to calculate the transferred electron number (n) per O2 molecule in the ORR process under different potential.

As for OER experiment, The LSV polarization data was recorded from 0.1~ 0.8 V (vs. Ag/AgCl) at the scan rate of 10 mV s^{-1} under 1,600 rpm rotating speed. AC impedance measurements of the catalysts were performed in the same configuration at the overpotential of 400 mV vs. Ag/AgCl from 100 kHz to 10 mHz with a VMP 3 electrochemical workstation in O$_2$-saturated 0.1 M KOH solution. For

chronoamperometric test, the catalyst were loaded on the carbon cloth and was also activated in O_2-saturated alkaline medium for 20 cycles, and then a static overpotential and current density were fixed for a certain time during continuous ORR and OER process to obtain the curve of time dependence of the current density and potential, respectively.

HER Activities of the Catalysts. With regard to HER experiment, all the experiments were conducted the same condition except the LSV polarization data was executed from -0.936 ~ -1.436V (vs. Ag/AgCl) at the scan rate of 5 mV s^{-1} under 1,600 rpm rotating speed in a 1M KOH.

Rechargeable Zinc-Air Battery Assembly and Tests. A custom-built rechargeable zinc-air battery was constructed, with a zinc plate anode and an electrocatalyst containing-cathode, connected by 6 M KOH and 0.2 M zinc acetate. The cathode was prepared by dropping the above catalyst inks onto the center area of carbon paper (1 cm in diameter) to achieve a loading of 1 mg cm^{-2}.

All-Solid-State Rechargeable Button Zinc-Air Battery Assembly. All as-prepared catalysts were loaded on the carbon cloth to use as the air cathodes and zinc plates were polished to be used as the anodes. The alkaline gel electrolyte was prepared by dissolving KOH, $Zn(CH_3COO)_2$ and PVA in deionized water at 90 °C under vigorous stirring until the solution became clear. All-solidstate zinc-air batteries were assembled by separating the air cathode and zinc anode with the alkaline gel polymer in button batteries with air vent.

Full Water Splitting System Assembly. Both the anode and cathode were prepared

by dropping the above catalyst inks onto the center area of carbon paper (1 cm in diameter) to achieve a loading of 1 mg cm^{-2}. The LSV was collected at a scan rate of 5 mV s^{-1} under the 1M KOH with iR corrected. And the chronoamperometric test were conducted after activated in O$_2$-saturated alkaline medium for 20 cycles, and then a static current densites was fixed for a certain time during continuous full water splitting process to obtain the curve of time dependence of the potentials.
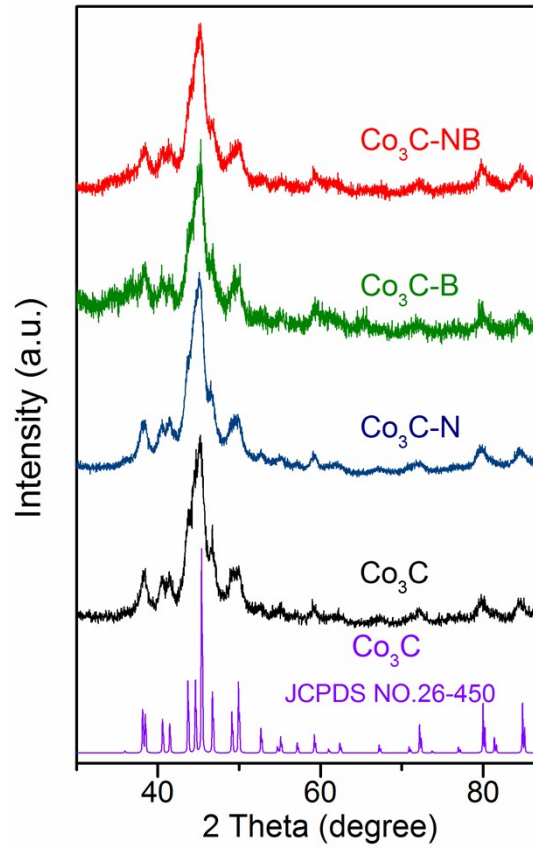
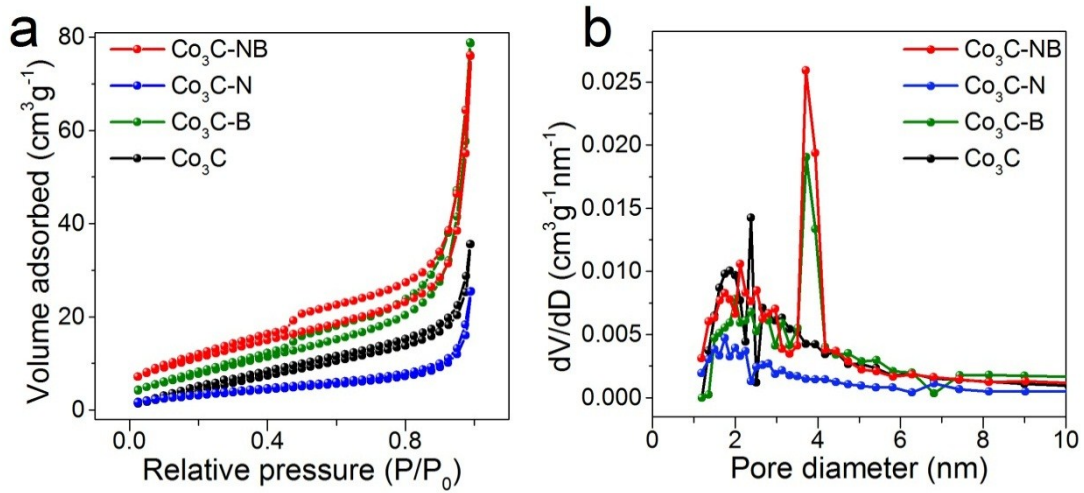**Figure S1** XRD patterns of Co_3C, Co_3C-N, Co_3C-B and Co_3C-NB.

Figure S2 (a, b) N_2 adsorption-desorption isotherm and the corresponding pore-size distribution of these materials.

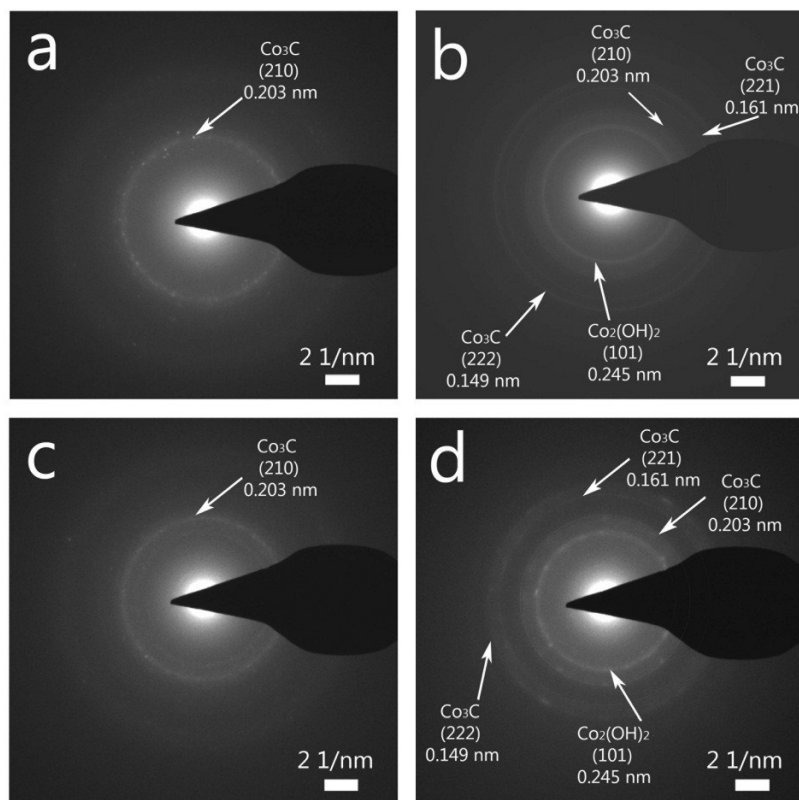**Figure S3** (a, b, c and d) SAED patterns of Co_3C, Co_3C-B, Co_3C-N and Co_3C-NB.
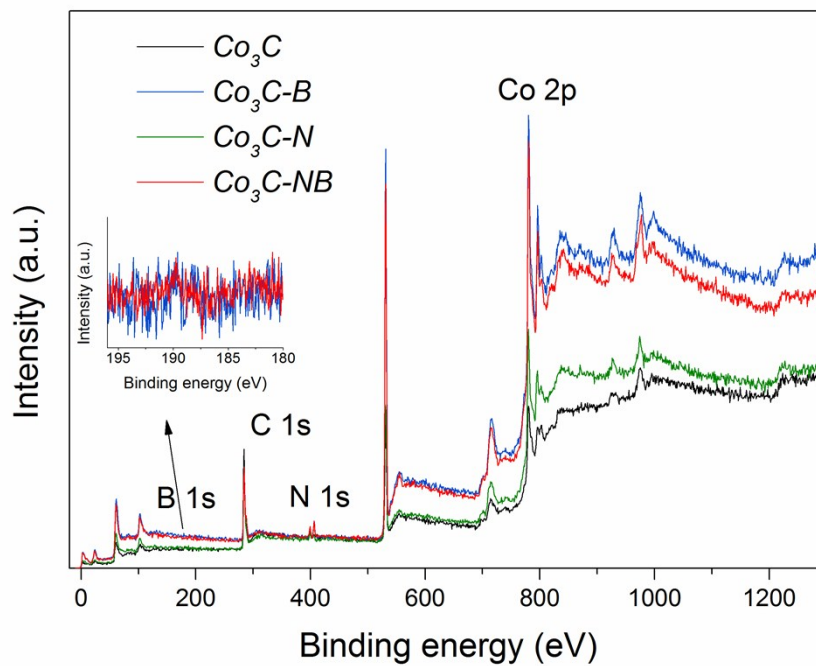
Figure S4 Survey XPS spectrums of Co_3C-based samples.
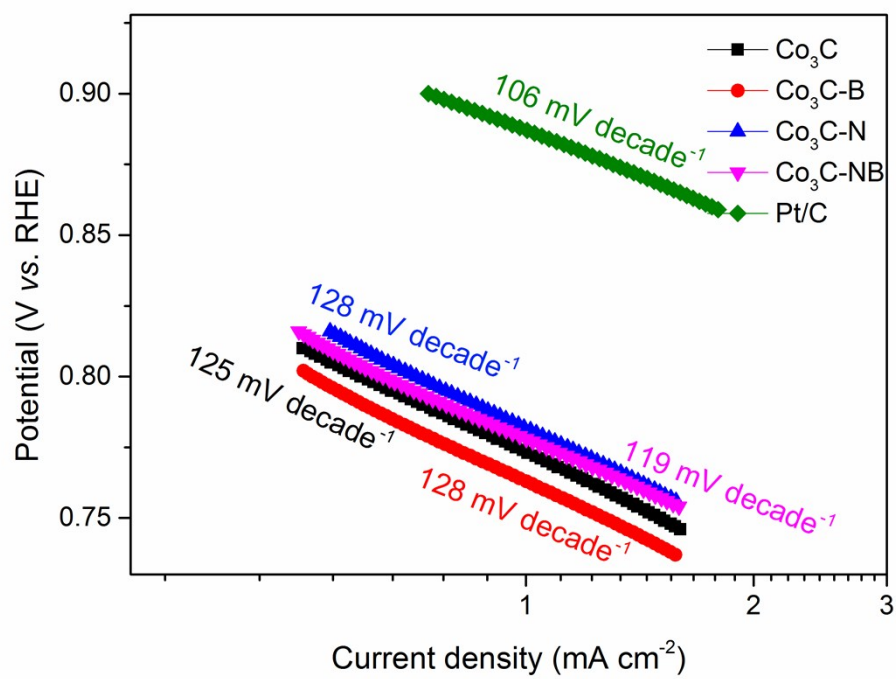
Figure S5 The corresponding Tafel plots of Co₃C-based samples toward ORR.
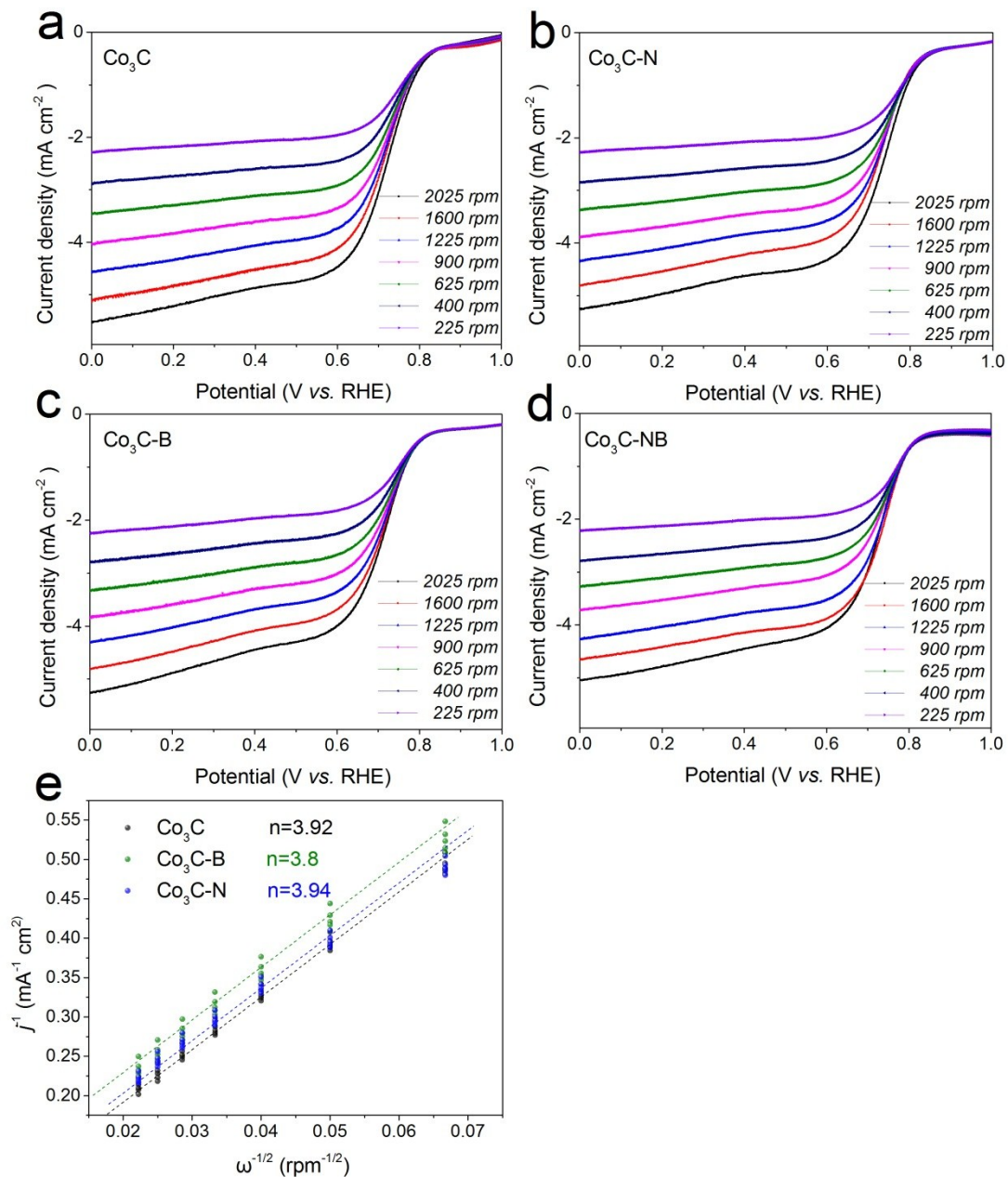
Figure S6 (a, b, c and d) The LSV curves at different scan rates. e) The corresponding transfer numbers (n) as calculated by the slope of Koutecky-Levich plots from the collected LSV data.
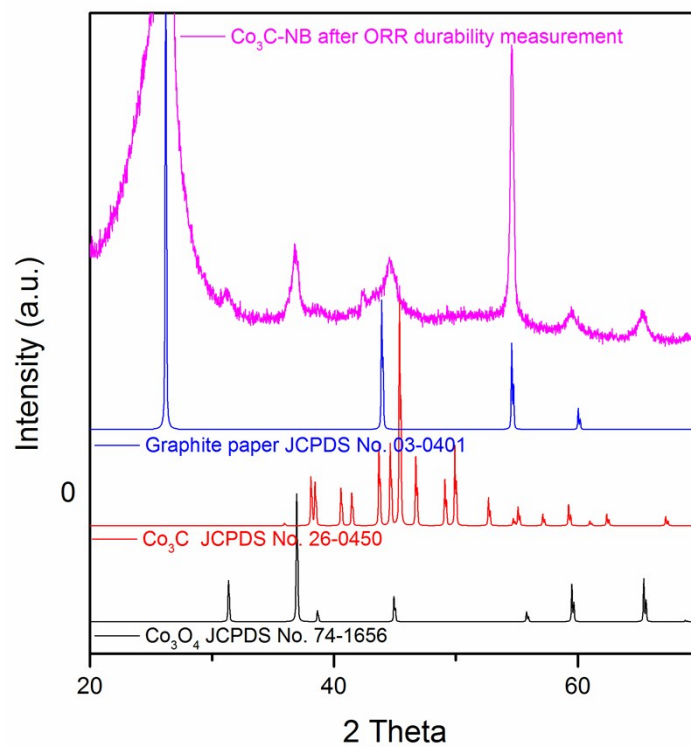
Figure S7 XRD pattern of Co$_3$C-NB after ORR durability measurement at 0.2 V vs. RHE for 4 hours.
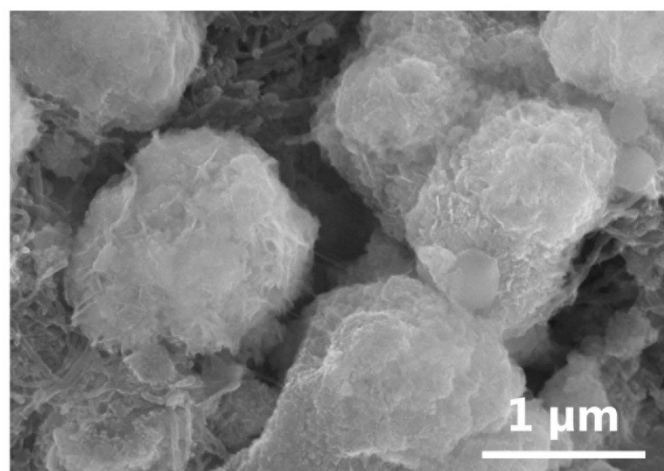
Figure S8 SEM image for Co$_3$C-NB after ORR stability test.
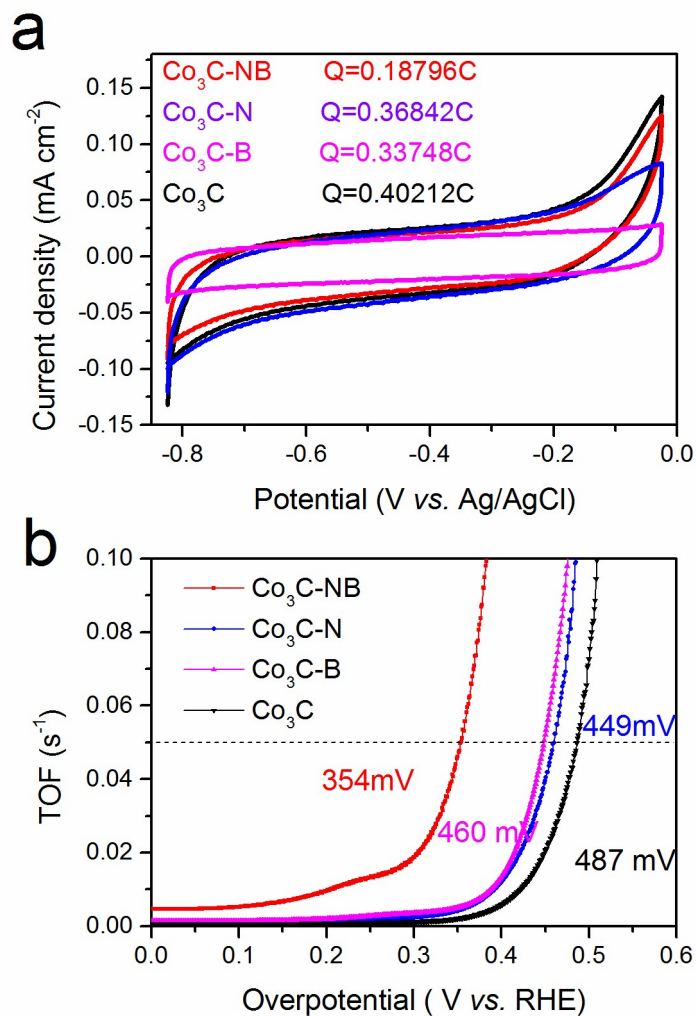
Figure S9 (a) Cyclic voltammetry cycling in phosphate buffer (pH = 7) with a scan rate of 50 mV s^{-1} range from- 0.8 to 0 V vs. Ag/AgCl. (b) TOF data.
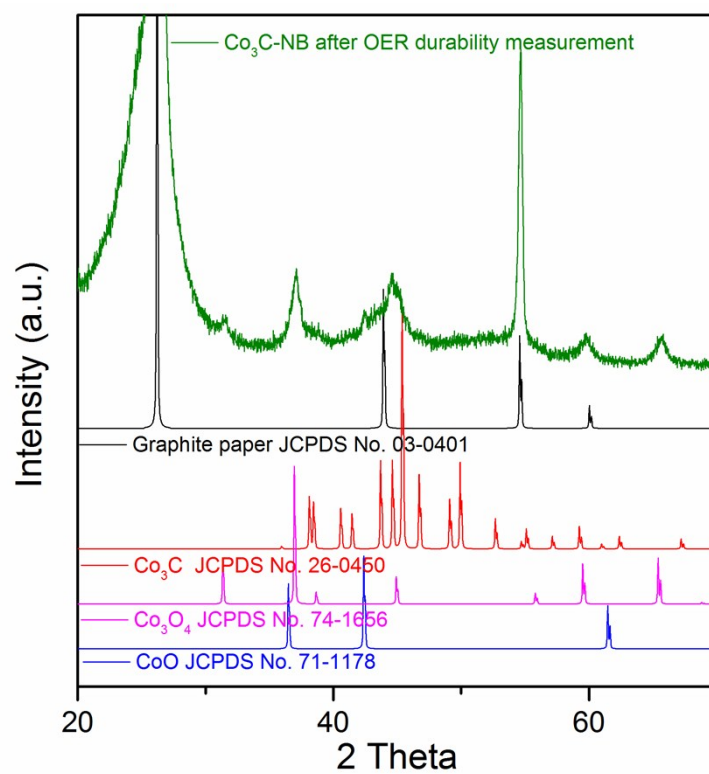
Figure S10 XRD pattern of Co₃C-NB after OER durability measurement at 0.2 V vs. RHE for 4 hours.
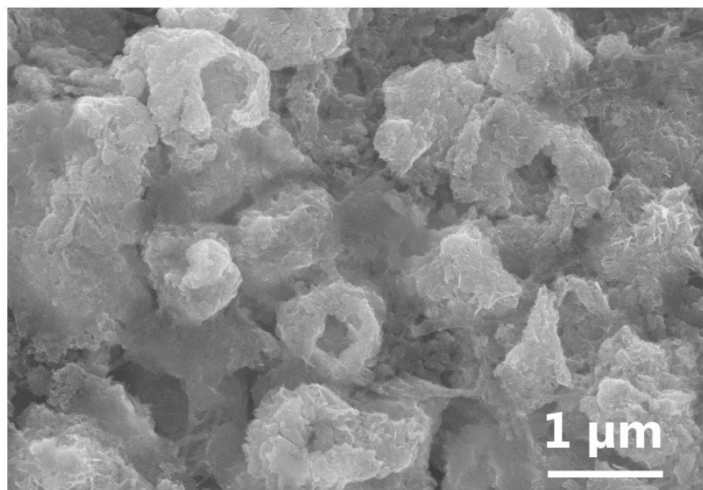
Figure S11 SEM images for Co$_3$C-NB after OER durable tests.
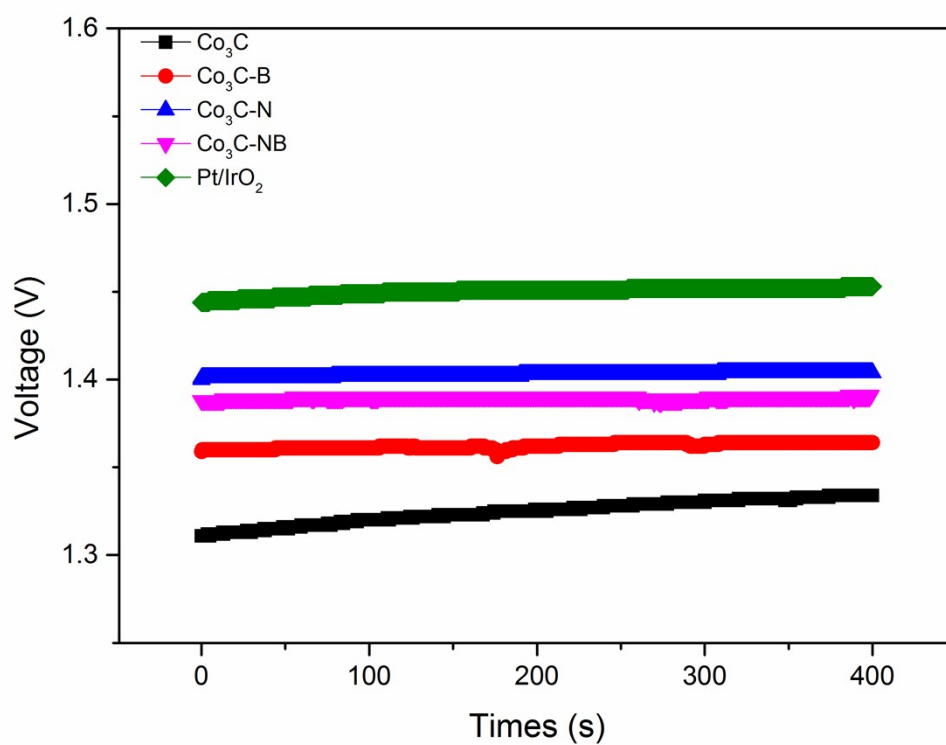
Figure S12 Open-circuit plots of rechargeable zinc–air batteries using Co$_3$C, Co$_3$C-N, Co$_3$C-B and Co$_3$C-NB and Pt/IrO$_2$ as air cathodes.
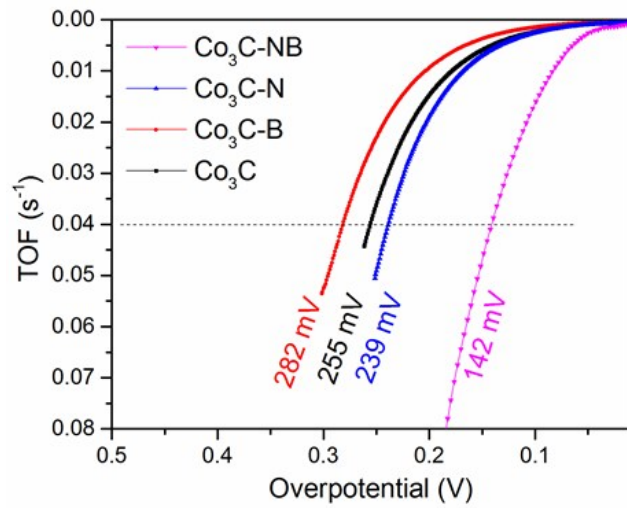
Figure S13 TOF data for HER of Co$_3$C-based samples.
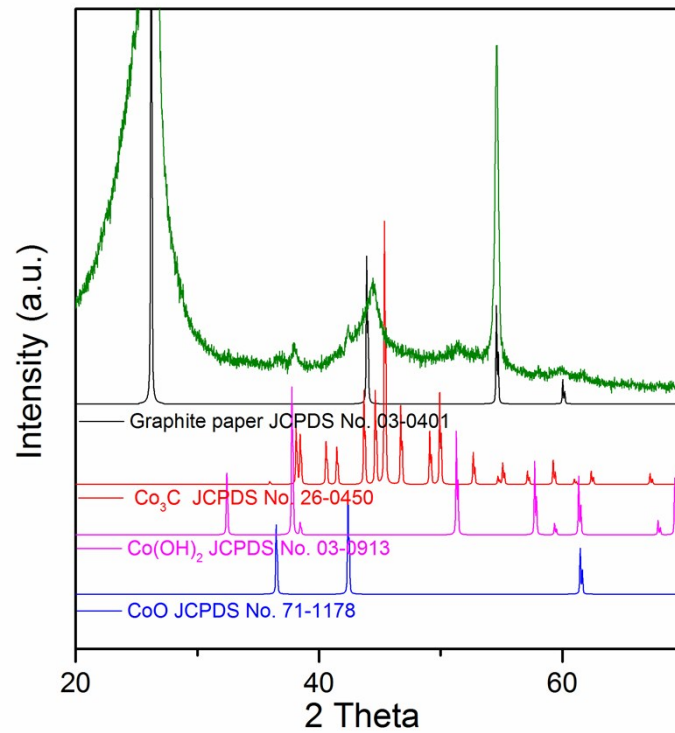
Figure S14 XRD pattern of Co$_3$C-NB after HER durability measurement at 0.2 V vs. RHE for 4 hours.
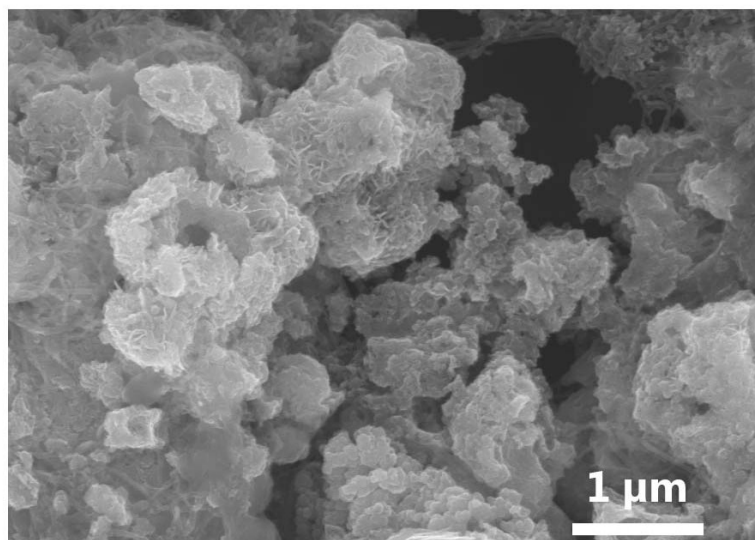
Figure S15 SEM image for Co$_3$C-NB after HER stability test.

Table S1 Content comparison of correspond elements of Co$_3$C, Co$_3$C-N, Co$_3$C-B and Co$_3$C-NB.

Element \\ Catalysts	Co 2p (at %)	C 1s (at %)	O 1s (at %)	N 1s (at %)	B 1s (at %)
Co$_3$C	55.53	16.74	27.73	–	–
Co$_3$C-N	63.35	10.56	24.61	1.48	–
Co$_3$C-B	67.67	4.57	27.76	–	–
Co$_3$C-NB	65.46	4.85	27.84	1.69	0.15

Table S2 The normalized contents for respect C and N species in Co$_3$C, Co$_3$C-N, Co$_3$C-B and Co$_3$C-NB.

Peak species			Co$_3$C		Co$_3$C-N		Co$_3$C-B		Co$_3$C-NB	
			Peak position	Normalized Species content	Peak position	Normalized Species content	Peak position	Normalized Species content	Peak position	Normalized Species content
C	1	Co-C	283.73	0.414	283.9	0.273	283.84	0.103	283.8	0.172
	2	C-C	284.4	0.276	284.4	0.335	284.4	0.467	284.4	0.393
	3	C-defect or pure C-N	285.5	0.124	285.94	0.15	285.5	0.218	285.94	0.083
	4	O-C/O=C-O	288.2	0.186	288.45	0.172	288.5	0.212	288.45	0.205
	5	Pure-C-N	-	-	287.32	0.028	-	-	287.32	0.044
	6	Pure-C-N	-	-	284.8	0.042	-	-	284.8	0.086
	7	B-C	-	-	-	-	-	-	282.8	0.017
N	1	Co-N$_x$ / Co-N$_x$-B	-	-	399.3	0.236	-	-	399.17	0.177
	2	Pyridinic-N	-	-	398.7	0.19	-	-	398.7	0.107
	3	Pyrrolic-N	-	-	400.15	0.1425	-	-	400.15	0.08
	4	Quaternary-N	-	-	401.2	0.0665	-	-	401.2	0.025
	5	Oxidized-N	-	-	403	0.0475	-	-	403	0.027
	6	Chemisorbed-N	-	-	406.3	0.3175	-	-	406.3	0.529
	7	B-N	-	-	-	-	-	-	397.4	0.055

Table S3 Comparison of ORR activity of our Co_3C-NB catalyst on glassy carbon electreode with those of the ORR catalysts reportedly previously.

Catalysts	Tafel slope (mV dec^{-1})	Electrolyte	loading	Halfwave potential	Refs.
Co_3C-NB		0.1 M KOH	0.353 mg cm^{-2}	0.748 V	This work
Meso-CoNC@GF	75.7	M KOH		0.87 V	1
Mesoporous Co_3O_4/ N-rGO Nanosheets	54	0.1 M KOH	1.28 mg cm^{-2}	0.79 V	2
NiFe-LDH/Co_xN-CNF	-	0.1 M KOH	0.12 mg cm^{-2}	0.79 V	3
Co_3O_4 nanocrystals on graphene		0.1 M KOH	0.24 mg cm^{-2}	0.83 V	9
Co_3C/VA-GNRs	45	0.1 M KOH	1.0 mg cm^{-2}	0.77 V	15
CoP@CC	-	0.1 M KOH		0.67 V	S1
FeCo+NPC		0.1 M KOH		0.58 V	17
Co/N/S-CNPs				0.87 V	18
Co_9S_8 (NS/rGO-Co)	74	0.1 M KOH		0.82 V	19
Co/CoOx Nanoshoots on Perovskite Mesoporous Nanofibres	-	0.1 M KOH		0.76 V	20
$Co_{0.85}$Se@NC		0.1 M KOH	0.4 mg cm^{-2}	Morethan 0.8 V	22
Co@NCNT	94.8	0.1 M KOH	0.425 mg cm^{-2}	0.828 V	23
Ni_1Co_4S@C-1000	-	0.1 M KOH	0.1415 mg cm^{-2}	0.60 V	24
15% PANI/ZIF-67		0.1 M KOH	0.6 mg cm^{-2}	0.73 V	25
Co_9S_8 HMs-140/C	-	0.1 M KOH	0.8 mg cm^{-2}	0.82 V	26
Fe_2P/Fe_4N@C-800	65	0.1 M KOH	0.3 mg cm^{-2}	0.82 V	27
$Ni_{0.75}$Se nanocrystal	-	1 M KOH	0.6 mg cm^{-2}	~0.74 V	28
Mo–N/C@MoS_2		0.1 M KOH	-	0.81 V	32
GO-PANi$_{31}$-FP		0.1 M KOH	-	< 0.75 V	33
Co_{15}–N–C800	62	0.1 M KOH	0.49 mg cm^{-2}	0.82 V	37
CoP@SNC		0.1 M KOH	0.6 mg cm^{-2}	0.79	44
N,B-codoped Defect-rich Graphitic Carbon	65	0.1 M KOH	0.255 mg cm^{-2}	0.835 V	47
Co-N_x-B_y-C carbon nanosheets	64	0.1 M KOH	0.5 mg cm^{-2}	0.83 V	48
Single-crystal CoO Nano Rods	47	1 M KOH	0.19 mg cm^{-2}	0.85 V	56
CoZn-NC-700	60	0.1 M KOH	0.24 mg cm^{-2}	0.84 V	64
$Co_3FeS_{1.5}(OH)_6$	96	0.1 M KOH		0.721 V	61

Table S4 Comparison of OER activity of our Co_3C-NB catalyst on glassy carbon electreode with those of the OER catalysts reportedly previously.

Catalysts	Tafel slope (mV dec^{-1})	Electrolyte	Loading	η (at 10mAcm^{-2})	Refs.
Co_3C-NB		0.1 M KOH	0.353 mg cm^{-2}	358 mV	This work
Meso-CoNC@GF	201	1 M KOH		430 mV	1
Mesoporous Co_3O_4/ N-rGO Nanosheets	54	0.1 M KOH	0.128 mg cm^{-2}	490 mV	2
NiFe-LDH/Co,N-CNF	60	0.1 M KOH	0.12 mg cm^{-2}	312 mV	3
Co_3O_4 nanocrystals/graphene	67	1 M KOH	0.24 mg cm^{-2}	310 mV	9
Co_3C particles				455 mV	16
CoP@CC	124		0.258 mg cm^{-2}	300 mV	S1
FeCo+NPC	70			360 mV	11
Co/N/S-CNPs	130	0.1 M KOH		370 mV	18
NS/rGO-Co_4	72	0.1 M KOH		265 mV	19
Co/CoO$_x$/perovskite mesoporous nanofibres		0.1 M KOH		410 mV	20
$Co_{0.85}$Se@NC	75	1 M KOH	0.4 mg cm^{-2}	320 mV	22
Co@NCNT	116	1 M KOH	0.425 mg cm^{-2}	429 mV	23
Ni1Co_4S@C-1000	64	0.1 M KOH	0.1415 mg cm^{-2}	240 mV	24
15% PANI/ZIF-67	37	0.1 M KOH	0.6 mg cm^{-2}	330 mV	25
Co_9S_8 HMs-140/C	113	0.1 M KOH	0.8 mg cm^{-2}	420 mV	26
Fe_2P/Fe_4N@C-800	177	1 M KOH	0.3 mg cm^{-2}	410 mV	27
$Ni_{0.5}$Se nanocrystal	51	1 M KOH	0.6 mg cm^{-2}	330 mV	28
Mo–N/C@MoS_2	72	0.1 M KOH		390 mV	32
GO-PANi$_{31}$-FP	136	0.1 M KOH		~570 mV	33
CoP@SNC	68	1.0 M KOH	0.6 mg cm^{-2}	350 mV	44
N,B-codoped Defect-rich Graphitic Carbon		0.1 M KOH	0.255 mg cm^{-2}	420 mV	47
Co-N$_x$-B$_y$-C carbon nanosheets	-	0.1 M KOH	0.5 mg cm^{-2}	430 mV	52
Co/NBC-900	70	1.0 M KOH		302 mV	51
Single-crystal CoO Nano Rods	44	1 M KOH	0.19 mg cm^{-2}	330 mV	56
Cobalt-defected $Co_{3-x}O_4$	38.2	1 M KOH		268 mV	S2
Plasma-engraved Co_3O_4 nanosheets	68	0.1 M KOH		300 mV	54
Co_2B nanoparticles		0.1 M KOH	0.2 mg cm^{-2}	371 mV	67
CoZn-NC-700	69	0.1 M KOH	0.24 mg cm^{-2}	390 mV	57

$Co_3FeS_{1.5}(OH)_6$	79	0.1 M KOH		358 mV	S3
Amorphous Co_2B-500/NG	45	0.1 M KOH	0.21 mg cm^{-2}	380 mV	66
$Mn_3O_4/CoSe_2$	49	0.1 M KOH	0.2 mg cm^{-2}	450 mV	S4
Co_9S_8/N-C hybrid	75	0.1 M KOH	0.8 mg cm^{-2}	650mV/33mA	S5
$CoS_2(400)$/N,S-GO	75	0.1 M KOH	0.528 mg cm^{-2}	390 mV	S6
N-Co_9S_8/graphene hybrid	82.7	0.1 M KOH	0.2 mg cm^{-2}	409 mV	S7

Table S5 Summary of Zn-air battery performance of catalysts used in this work.

	Charge (V)	Discharge (V)	Band gap (V)	Efficiency
Co_3C	2.03	1.0733	0.9567	52.9%
Co_3C-N	2.0126	1.1288	0.8838	56.1%
Co_3C-B	2.0669	1.0956	0.9713	53%
Co_3C-NB	1.9959	1.1269	0.869	56.5%
Pt/C+ IrO_2	2.0263	1.2162	0.8101	60%

Table S6 Summary of multi-functional activity of the Co-based and other catalysts in literatures.

	Loading (mg cm^{-2})	ORR		OER		Zn-air batteries			Refs.
		$E_{1/2}$ (V)	Durability Time/current density	$E_{j=10}$ (V)	Durability Time/current density	ΔE ($E_{j=10}$-$E_{1/2}$) (V)	Power density (mW cm^{-2})	Durability Time/current density	
Co$_3$C-NB	*0.353*	*0.748*	*12h /0.2V vs.RHE*	*1.588*	*12h /50 mA cm^{-2}*	*0.84*	*45.4*	*180 h /5 mA cm^{-2} (custom-built zinc–air batteries) 13 h /20 mA cm^{-2} (All solid state batterials)*	*This work*
CoP@CC	0.258	0.67	10h /10 mA cm^{-2}	1.53	27.7h /10 mA cm^{-2}	0.86	~30	10h /10 mAcm^{-2}	[S1] 2017
FeM/NPC (M=Co, Ni)	0.485	0.78	~25h /10 mA cm^{-2}	1.59	~25h /10 mA cm^{-2}	0.81	-	25h /25 mA cm^{-2}	[17] 2017
Co/N/S-CNPs	0.275	0.87		1.6		0.73	96	40h /5 mA cm^{-2}	[18] 2018
Co$_9$S$_8$ (NS/rGO-Co)	0.485	0.82	10h /93.5%	1.52	10h /76%	0.7	-	-	[19] 2017
Co/CoO$_x$ nanoshoots		0.76	12h /~ 100%	1.62	12h /~ 95%	0.86	-	-	[20] 2017
Co$_{0.85}$Se@NC	0.4	~0.82	12h /~ 90% / 0.672 V	1.55	12h /~ 93.4% /50 mA cm^{-2}	0.8	268	30h /10 mA cm^{-2}	[22] 2017
Co@NCNT	0.425	0.828	3.5h /~ 80% / 0.8 V	1.659	-	0.831	138.82	16.5 h / 10 mA cm^{-2}	[23] 2016

Ni1Co$_4$S@C-1000	0.1415	0.6	-	1.51	2h /~ 90% / 1.6 V	0.92	-	-	[24] 2016
PANI/ZIF-67	0.6	0.75	1.5h /~ 100% / 0.5 V	1.56	-	0.83	45	-	[25] 2017
Co$_9$S$_8$ HMs-140/C	0.8	0.82	-	1.65	-	0.83	-	-	[26] 2017
Fe$_2$P/Fe$_4$N@C-800	0.3	0.8	-	1.64	2000 CV cycles /10 mV overpotential higher	0.84	-	-	[27] 2017
Ni$_x$Se (0.5 ≤ x ≤1)	0.6	~0.75	-	1.56	10h /~ 98% /10mA cm^{-2}	-	-	200cycles /10 mA cm^{-2}	[28] 2018
Surface Oxidation of AuNi Heterodimers	0.186	0.73	-	1.58	3h /~ 120% /440 mV overpotential	0.85	-	-	[29] 2018
N, B-codoped Defect-rich Graphitic Carbon Nanocages	0.255	0.835	-	1.65	-	0.815	320	14h /10 mA cm^{-2}	[47] 2017

Table S7 Comparison of HER activity of our Co_3C-NB catalyst on glassy carbon electreode with those of the HER catalysts reportedly previously.

Catalysts	Tafel slope (mV dec^{-1})	Electrolyte	Loading	η (at 10mAcm^{-2})	Refs.
Co_3C-NB	119	0.1 M KOH	0.353 mg cm^{-2}	154 mV	This work
FeCo+NPC	125	-	-	340 mV	17
Co/N/S-CNPs	108	1 M KOH	-	240 mV	18
NS/rGO-Co$_4$	-	0.1 M KOH		193 mV	19
Co/CoO$_x$/perovskite mesoporous nanofibres	-	1 M KOH	-	~220 mV	20
Co$_{0.85}$Se@NC	125	1 M KOH	0.4 mg cm^{-2}	230 mV	22
Co@NCNT	93	0.1 M KOH	0.425 mg cm^{-2}	~250 mV	23
15% PANI/ZIF-67	123		0.6 mg cm^{-2}	>350 mV	25
Co$_9$S$_8$ HMs-140/C	108	0.1 M KOH	0.8 mg cm-2	250 mV	26
Fe$_2$P/Fe$_4$N@C-800	130	0.5 M H$_2$SO$_4$	0.3 mg cm^{-2}	232 mV	27
Ni$_{0.75}$Se	86	1 M KOH	-	233 mV	28
Mo–N/C@MoS$_2$	64.3	1 M KOH	-	117 mV	32
GO-PANi$_{31}$-FP	-	0.1 M KOH	-	520 mV	33
N-Co@G	98	0.1 M KOH	-	337 mV	38
CoP@SNC	82	1.0 M KOH	0.6 mg cm^{-2}	174 mV	44
N,B-codoped Defect-rich Graphitic Carbon	82.1	0.5 M H$_2$SO$_4$	0.383 mg cm^{-2}	175.3 mV	47
Co/NBC-900	146	1.0 M KOH	-	117 mV	51
CoNi nanoalloy/graphene	104	Acidic electrolyte	0.32 mg cm^{-2}	224 mV	59
CoO$_x$@CN	115	1 M KOH	0.42 mg cm^{-2}	232 mV	64
NG@Co-MMT	-	0.5 M H$_2$SO$_4$	-	210 mV	73
Co@BCN	73.2	1 M KOH	1.5 mg cm^{-2}	183 mV	76

Co-NRCNTs	-		0.28 mg cm^{-2}	260 mV	S8
FeCo@NCNTs	-		0.32 mg cm^{-2}	276 mV	S9

REFERENCES

(S1) Y. F. Cheng, F. Liao, W. Shen, L. B. Liu, B. B. Jiang, Y. Q. Li and M. W. Shao, *Nanoscal*e, **2017**, *9*, 18977.

(S2) R. R. Zhang, Y. C. Zhang, L. Pan, G. Q. Shen, N. Mahmood, Y. H. Ma, Y. Shi, W. Y. Jia, L.Wang, X. W. Zhang, W. Xu and J. J. Zou, *ACS catal.,* **2018**, *8*, 3803.

(S3) H. F. Wang, C. Tang, B. Wang, B. Q. Li and Q. Zhang, *Adv. Mater.,* **2017**, *29*, 1702327.

(S4) M. R. Gao, Y. F. Xu, J. Jiang, Y. R. Zheng and S. H. Yu, *J. Am. Chem. Soc.,* **2012**, *134*, 2930.

(S5) X. C. Cao, X. J. Zheng, J. H. Tiana, C. Jina, K. Keb and R. Z. Yang, *Electrochim. Acta,* **2016**, *191*, 776.

(S6) P. Ganesan, M. Prabu, J. Sanetuntikul and S. Shanmugam, *ACS Catal.,* **2015**, *5*, 3625.

(S7) S. Dou, L. Tao, J. Huo, S. Y. Wang and L. M. Dai, *Energy Environ. Sci.,* **2016**, *9*, 1320.

(S8) X. Zou, X. Huang, A. Goswami, R. Silva, B. R. Sathe, E. Mikmeková, T. Asefa, *Angew. Chem.,* **2014**, *126*, 4461.

(S9)J. Deng, P. J. Ren, D. H. Deng, L. Yu, F. Yang and X. H. Bao, *Energy Environ. Sci.,* **2014**, *7*, 1919.